

2D Boron Nitride Heterostructures: Recent Advances and Future Challenges

Junkai Ren and Plinio Innocenzi*

Hexagonal boron nitride (h-BN) is one of the most attractive 2D materials because of its remarkable properties. Combining h-BN with other components (e.g., graphene, carbonitride, semiconductors) to form heterostructures opens new perspectives to developing advanced functional devices. In this review, the state-of-the-art in h-BN heterojunctions is highlighted. The preparation of high-quality 2D h-BN structures with fewer defects can maximize its intrinsic properties, such as thermal conductivity and electrical insulation, which are particularly important in 2D van der Waals electronics. On the other hand, the controlled introduction in 2D h-BN of multiple defects creates new properties and advanced functions. In this last case, only through a better understanding of the nature and function of defects, it is possible to develop advanced applications based on h-BN heterostructures. Engineering of the heterojunctions, such as the design of bonding at the interfaces, also plays a primary role. Several applications are proposed for h-BN heterostructures, mostly in sensing and photocatalysis, and some new perspectives worth further studies are opened. Finally, the current challenges and the rising opportunities for the future developments of next-generation h-BN heterostructures are discussed.

1. Introduction

Since the first isolation of graphene from graphite, 2D materials have immediately opened new exciting perspectives in materials science and engineering.^[1] Hexagonal boron nitride (h-BN), in particular, which has a layered structure similar to graphene, has attracted much attention because of its unique combination of properties. B–N bonds with sp^2 hybridization and a slight ionic character, in comparison to the covalent C–C bond of graphite, characterize h-BN.^[2] At the same time, van der

Waals forces govern the interplane interaction, such as in graphite.


h-BN nanostructures preserve their thermal stability up to 1000 °C and oxidize in the 1000–1200 °C range, forming B_2O_3 . The oxidation process in h-BN nanosheets is observed, in general, at lower temperatures, starting from 850 °C.^[3] h-BN monolayers have a high thermal conductivity up to 751 W mK⁻¹ at 25 °C and high electrical insulation^[4]; this combination of properties makes 2D h-BN an excellent candidate for heat dissipation in electronic devices. Experimental and theoretical studies have shown that h-BN has a wide energy gap (E_g), around 6 eV,^[5] and several optics, electronics, and electro-optics applications based on this property have been envisaged.^[6]

h-BN can be formed in a large variety of different nanostructures from 3D to 0D, such as monolayers, nanoribbons, nanotubes, nanodots, nanocages, and fullerene-like molecules.^[7,8] In particular, h-BN

can be easily exfoliated from bulk crystals down to few layers or deposited as monolayer using different methods.^[9] h-BN nanosheets have been obtained by developing both top-down and bottom-up routes even if controlling the number of layers, their dimension and the formation of defects remains a technological challenge.

Fabrication of high-quality h-BN layers with few defects allows full exploitation of the intrinsic properties of 2D h-BN, especially for developing electronic and optoelectronic devices.^[10,11] Although obtaining a less-defective h-BN layer is an important technological task, several of the functional properties of h-BN in the 2D form depends on the presence of defects, which can be of different nature.^[12,13] Furthermore, multiple defects can co-occur, such as carbon, oxygen and hydrogen impurities, boron/nitrogen vacancies.^[14] The defects are also not homogeneously distributed in the material, while the edges also play a primary role because of dangling bonds. Most of the h-BN optical properties depend on defects but achieving their strict control remains very difficult, especially in 2D structures obtained via exfoliation processes. Several methods for inducing functional properties in h-BN layers rely on the formation of defects. One of the main strategies is creating structural “holes” in the layers to promote dangling bonds. The process has, however, several limitations in terms of reproducibility and control of the material properties.

J. Ren, P. Innocenzi
Department of Chemistry and Pharmacy
Laboratory of Materials Science and Nanotechnology
CR-INSTM
University of Sassari
Via Vienna 2, Sassari 07100, Italy
E-mail: plinio@uniss.it

 The ORCID identification number(s) for the author(s) of this article can be found under <https://doi.org/10.1002/ssr.202100068>.

© 2021 The Authors. Small Structures published by Wiley-VCH GmbH. This is an open access article under the terms of the Creative Commons Attribution License, which permits use, distribution and reproduction in any medium, provided the original work is properly cited.

DOI: 10.1002/ssr.202100068

The correlation between emission and defects has been the subject of several theoretical and experimental investigations. A defect-free h-BN crystal does not display any emission and has a sharp band-to-band absorption edge, whereas defects give rise to fluorescence.^[8] Point defects, for instance, are the source of single-photon emissions, and the discovery of this property has promoted the design of quantum emitters in a wide range of energies.^[6,15]

The formation of heterojunctions based on 2D materials is a recent hot research topic, especially for the expected advantages in improving the performances of photocatalytic and sensing devices.^[16,17] The possibility of fabricating h-BN based heterostructures has increased the theoretical and experimental understanding for efficient integration of h-BN in advanced functional devices.^[18,19]

Combining different materials to form h-BN based heterostructures requires developing specific synthesis to control the interface bonding. Matching h-BN nanosheets with other materials allows forming heterostructures with fundamentally novel optical and electronic characteristics.^[1,20,21] Specifically, the as-synthesized h-BN materials, which are always negatively charged, can become carrier acceptors in a heterojunction improving the charge carrier separation in photocatalysis.^[22–24] Moreover, the large specific surface area of nanoscale h-BN and the polarity of B–N bonds would enable the formation of heterostructures with a larger number of active sites.^[25–27] The good thermal conductivity of h-BN favors heat dissipation and reduces heat-induced damage in heterojunctions.^[28,29] Furthermore, h-BN layers are an outstanding encapsulant and gate dielectric for hetero-bilayers in van der Waals 2D materials.^[6,30] In addition to the contribution of h-BN, the hetero-counterpart can also enhance some h-BN properties such as quantum emitting and optical sensing.^[15,31]

In this review, we have discussed the most recent advances in the experimental and theoretical studies about h-BN heterojunctions from the synthesis to the engineering of different functional applications. To describe the different heterostructures, we used composition rather than structural architecture as a criterion. The current challenges in the field have also been critically discussed.

2. Boron Nitride–Metal Compound Heterostructures

2.1. Boron Nitride–Titania Heterostructures

Titania (TiO₂) is the most common semiconductor employed in photocatalysis because of the excellent photoresponse, extensive availability, and low cost.^[32] The fast electron–hole pair recombination rate, however, represents an intrinsic limitation of the efficiency during photocatalysis. Moreover, different strategies to increase the titania performances, including the fabrication of functional heterojunctions, have been elaborated. Several authors claim that the photocatalytic activity of TiO₂ enhances by incorporating h-BN sheets to form a heterostructure-cocatalyst.^[33,34] However, much care is necessary to evaluate the performances of these heterojunctions. Bare 2D h-BN does not show any photocatalytic activity, which is, therefore, depending on defects.^[35] A clear understanding of the defect–property

relationship requires, as we have seen, precise control of defects in h-BN materials. Other 2D materials, such as tungsten disulfide (WS₂) and molybdenum disulfide (MoS₂), have a high intrinsic photocatalytic activity, and they remain the first choice for this type of application.^[36,37]

The interface plays a primary role in constructing heterojunctions because the formation of mixed bonds affects the material performances significantly. An example is the growth of titania nanoparticles on h-BN nanosheets, which can form Ti–O–B or Ti–B bonds at the interface. In general, tetrabutyl titanate is a feasible precursor to grow titania nanoparticles on h-BN nanosheets via controlled sol–gel processing.^[22] Through this process, TiO₂ nanoparticles with a diameter of around 10 nm have homogeneously grown on an h-BN nanosheet surface; the anatase titania phase forms after thermal treatment at 500 °C. The XPS data indicate the formation of mixed B–O–Ti bonds at the h-BN/TiO₂ interface, responsible for the tight binding of the two phases. The mixed bonding accelerates the transfer rate of photogenerated electrons. Hence, the photodegradation reaction rates of the h-BN–TiO₂ heterostructure are 3.6 and 4.2 times higher than the single-phase TiO₂, when rhodamine B (RhB) and methylene blue (MB) are used as test molecules.^[22]

A similar approach has been applied to form TiO₂ nanoparticles on the surface of porous and nonporous h-BN sheets.^[33] Porous h-BNs have been obtained by annealing in a tube furnace at 1100 °C for 2 h under H₂/N₂ (15 vol% hydrogen) gas flow, a mixture of boron trioxide and guanidine hydrochloride as the boron and nitrogen sources, respectively.^[38] The gas released by decomposition at a high temperature of guanidine hydrochloride produces holes in the h-BN structure with a dimension of 20–100 nm. The porous h-BN nanosheets improve the photocatalytic response of TiO₂, whereas the nonporous h-BNs gives a negligible contribution. The authors have attributed the enhanced performance to the excellent dispersion of TiO₂ nanoparticles on h-BN sheets (see **Figure 1a,b**), and, in particular, to the formation of B–O–Ti bonds between the boron dangling bonds at the open edges of the pores in h-BN nanosheets and the titania nanoparticles (**Figure 1c,d**). The B–O–Ti bonds promote an effective separation of the photo-generated electrons and holes, reducing thus the recombination rate (**Figure 1e**).^[33]

Another type of h-BN/TiO₂ heterostructure has been obtained using fluorinated h-BN nanosheets (F-BNs) synthesized via a two-step mechanochemical route.^[39] F-BN/TiO₂ composites have been prepared using TiCl₄ as the titania precursor.^[34] Fluorine, as a highly electronegative element, not only negatively charges the h-BN surface but also reduces its band gap to 4.1 eV, enabling a strong electrostatic interaction via the heterointerfaces of F-BN and TiO₂ nanoparticles. Hence, the F-BN/TiO₂ heterojunctions are characterized by higher absorption, strong electrostatic interaction, and enhanced photocatalytic degradation of RhB and MB even under visible light.^[34]

Ball-milling methods usually provide a high-intensity mechanical shear, which can exfoliate the bulk h-BNs and create nanocomposite structures directly.^[16] The method has been applied to produce h-BN nanosheets^[40] and fabricating heterostructures by adding together bulk h-BNs and commercial TiO₂^[41] into a ball-mill system. h-BN/TiO₂ heterostructures are finally obtained after a drying process. The milling process produces defective structures with N triangle defects (**Figure 2**), which negatively

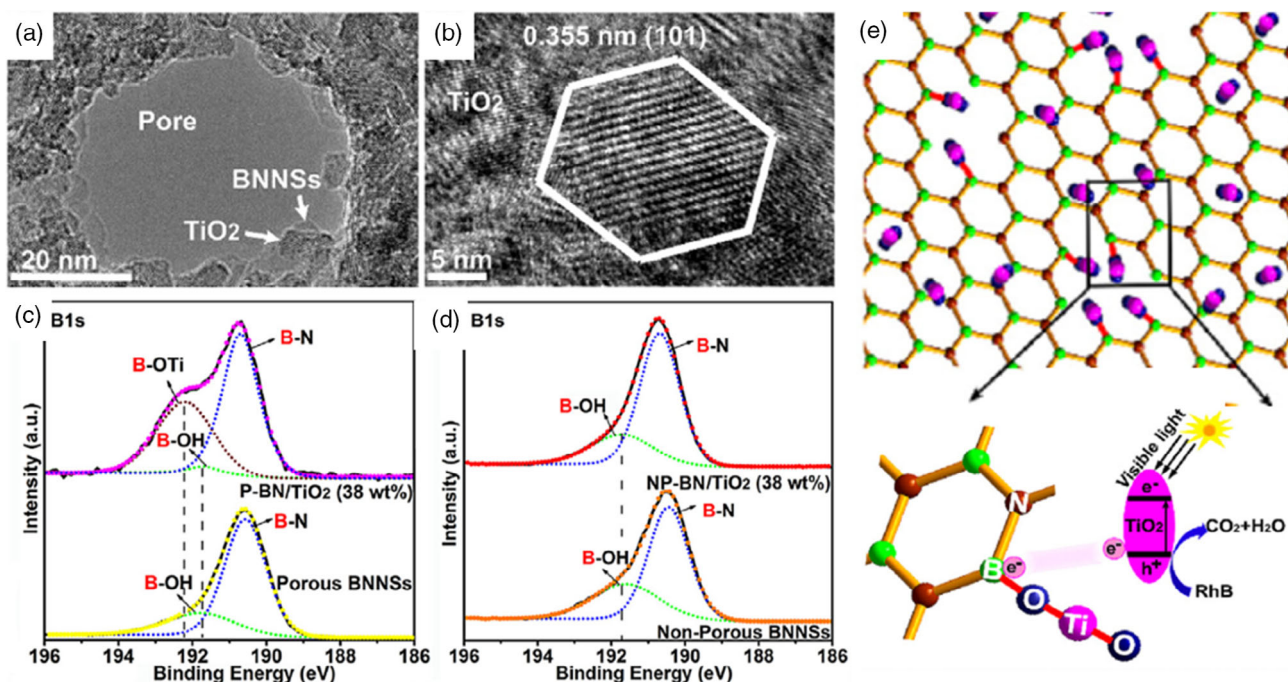


Figure 1. Example of a h-BN/TiO₂ heterostructure. a,b) TEM images of porous h-BN nanosheets and TiO₂ nanoparticles. c,d) XPS B1s spectra of porous and nonporous h-BN nanosheets, as well as their TiO₂-hybrids. e) Schematic diagram for the photocatalytic effect of porous h-BNs/TiO₂ heterostructure. Reproduced with permission.^[33] Copyright 2017, Elsevier.

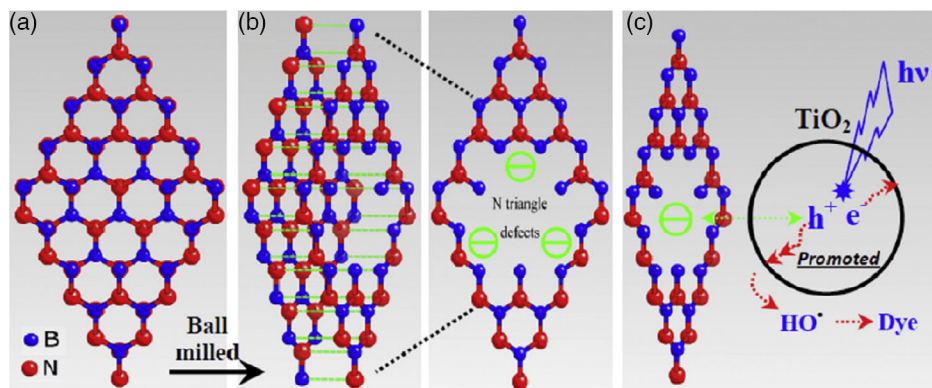


Figure 2. Schematic diagrams of: a) and b) the cleavage of h-BN and the structure of N edged triangle defects caused by the ball milling process, and c) the mechanism of the enhanced photocatalytic activity. Reproduced with permission.^[41] Copyright 2012, Elsevier.

charge the h-BN material increasing at the same time the contact area with the oxide. The negative charge has an important effect on the composite properties because it serves as a hole-transfer promoter and attractive or repulsive site for charged dyes adsorption.^[41]

These h-BN heterostructures are mainly realized using TiO₂ particles in micro- or nano scale.^[22,33,41–43] However, the recent classification of the European Union has listed titania powders as a category 2 carcinogen by inhalation, severely limiting the applications of titania particles. A possible alternative is synthesizing and using titania in the form of thin films. A template-assisted self-assembly process has been used to incorporate h-BN sheets into a mesoporous ordered titania thin film. A large photoactive

area characterizes the mesoporous films, together with an ordered and open porosity, and 2D materials can be incorporated in one-pot process without disrupting the self-assembly.^[44]

Two types of h-BN sheets, with and without defects respectively (oxygen-related and hydroxyl), have been used.^[35] The incorporation of 2D h-BN nanosheets does not damage the order and dimension of the mesopores (**Figure 3a–c**). The role of defects has been highlighted by an enhanced photodegrading activity under UV light irradiation, whereas the defect-free h-BN sheets show a negligible effect (**Figure 3d–f**). The presence of h-BN in the precursor sol promotes the anatase crystallization via heterogeneous nucleation while the defective species improves the light absorption in the UV region.^[35]

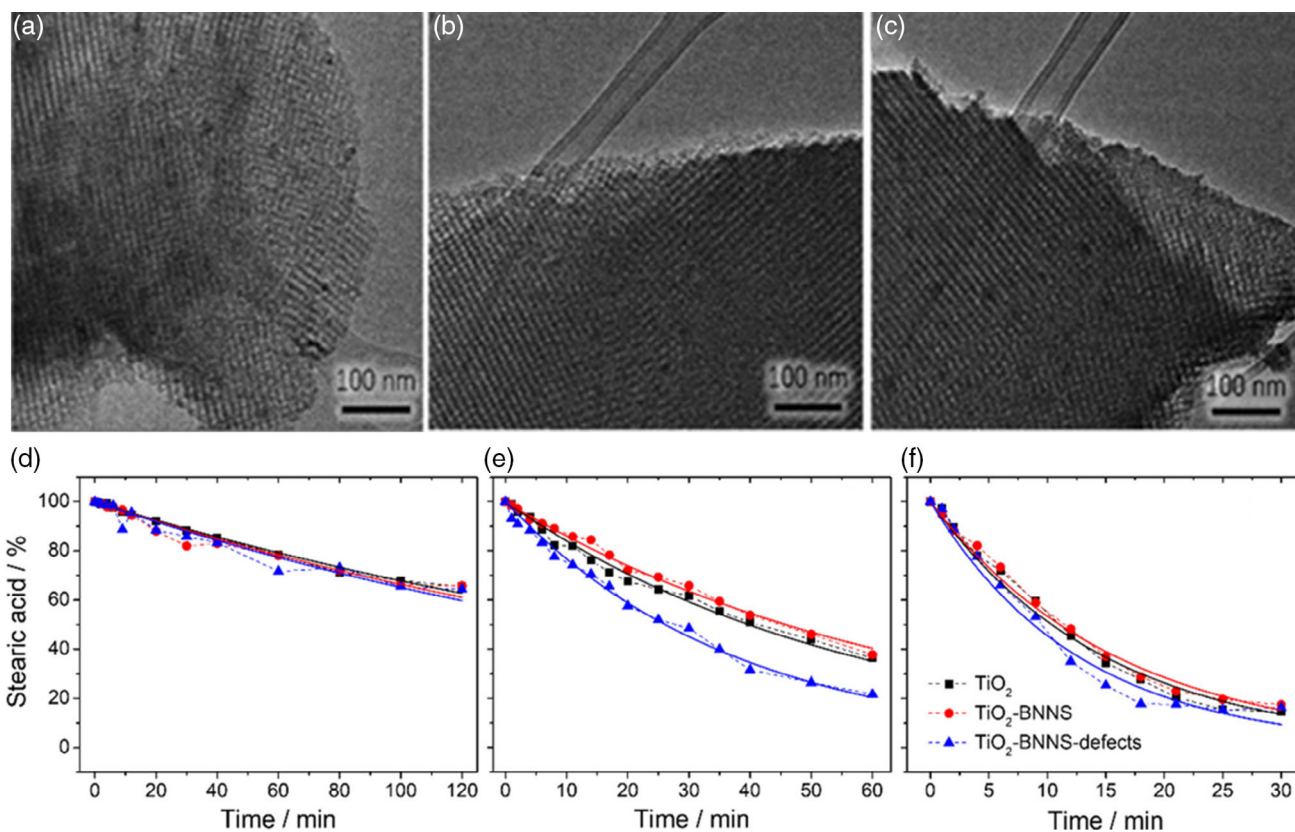


Figure 3. TEM images of films treated at 350 °C: a) TiO₂, b) TiO₂-BNNS, and c) TiO₂-BNNS defects. Photodegradation of stearic acid onto h-BN-TiO₂ films treated at d) 300, e) 350, and f) 400 °C, respectively. Reproduced with permission.^[35] Copyright 2021, American Chemical Society.

h-BN/TiO₂ heterostructures have also been tested for the photocatalytic generation of H₂. Porous BN sheets have been obtained via a bottom-up method by thermal heating boric acid and urea at 900 °C in N₂ gas. The h-BN/TiO₂ heterostructures have been prepared by dispersing the porous BN sheets into a solution of titanium isopropoxide in ethanol.^[45] After evaporating the solvent, the final annealing process at 700 °C in H₂ gas produces a disorder-engineered black hybrid with the formation of a Ti–B chemical interface. The Ti–B bonds enhance both UV and visible light absorption, promoting interfacial electron transfer. The h-BN-TiO₂ samples exhibit a photocatalytic H₂ production activity without the need for metal cocatalysts.^[45,46]

Another example is incorporating h-BN/TiO₂ composites into an epoxy resin (ER) to improve its mechanical performances. The wear rate of ER composite coatings decreases by 65.8% in comparison to the pristine ones.^[47] Furthermore, h-BN reduces the friction while TiO₂ increases the EP hardness, hence the synergic effect enhances the tribological performance of the nanocomposites.^[47]

Shanmugam et al. have covered h-BN plates with TiO₂ particles by spin-coating following annealing.^[48] In the h-BN-coated TiO₂ heterojunctions, the layered h-BN becomes an insulator and produces surface passivation of TiO₂, which can be used in dye-sensitized solar cells (DSSCs). A ≈57% improvement in the photo-conversion efficiency of DSSCs containing h-BN coatings, with respect to pristine titania,

has been measured. The h-BN passivation effectively reduces electron–hole carriers recombination at the TiO₂/dye/electrolyte interfaces.^[48]

h-BN/TiO₂ structures have also been produced in the shape of fibers. For example, Nasr et al. have prepared h-BN/TiO₂ nanofibers by electrospinning using different amounts of h-BN.^[49] The composite fibers have applied in photocatalysis and for the photodegradation of dyes, ibuprofene and organic contaminants in wastewater.^[50]

2.2. Boron Nitride–Zinc Oxide Heterostructures

Zinc oxide (ZnO) is a member of the II–VI semiconductor group with a wide bandgap (≈3.37 eV) and high exciton energy (≈60 meV).^[51] Different h-BN/ZnO heterostructures–heterojunctions have been explored to improve the ZnO functional performances. Fu et al. have prepared h-BN/ZnO heterostructures through a ball-milling process which induces the formation of negative charges in h-BN. The BN sheets serve as hole-transfer promoters and attractive–repulsive sites for the adsorption of charged dyes in a process that is analogous to what observed in h-BN/TiO₂ heterostructures.^[52] The composites have been used to test the photodegradation of RhB and MB under UV-light, which resulted in more efficiency with respect to the ZnO bare samples. The h-BN loading in the ball milling

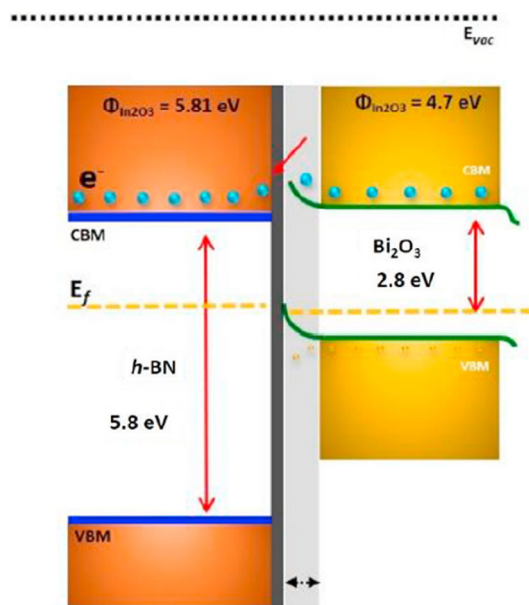
processing of ZnO is another key factor for controlling the heterojunction properties, with a maximum efficiency observed with 1.0 wt% h-BN loading.^[52]

Achieving a good absorption of CO₂ gas at the low pressure of 1 bar is still challenging. 3D h-BN/ZnO heterostructures functionalized by -NH₂ groups have shown an efficient CO₂ capture efficiency at 1 bar and 273 K.^[53] The composite has been prepared via a two-step process (Figure 4); in the first one, NH₂-functionalized h-BN sheets have been obtained by ball-milling bulk BNs with urea; in the second step (Step 2, II, in Figure 4), 3D spherical-porous h-BN/ZnO superstructures finally form via evaporation-induced solvothermal synthesis and annealing. The spherical h-BN/ZnO material has shown a high capacity of CO₂ capturing and good reusability. The high chemisorption is due to van der Waals interaction and H bonds from the surface of ZnO and the in-plane and edged amino groups in the amine-functionalized h-BN nanosheets.

2D h-BN-doped ZnO thin films have been deposited onto different types of substrates such as glass, ITO and FTO oxide-coated glass, via thermionic vacuum arc (TVA) processing.^[54] The film growth is directly affected by the substrate with a shift in the ZnO bandgap.

2.3. Boron Nitride–Bismuth Heterostructures

Bismuth (Bi), and in particular Bi³⁺ based semiconductors, are characterized by a photoresponse in the visible range because of the hybridization of the valence bands of O 2p and Bi 6s² orbitals.^[55] The stable α -phase of bismuth oxide (Bi₂O₃), particularly, is a p-type semiconductor with a bandgap of around 2.8 eV, making it a suitable catalyst for electrochemical sensing. An h-BN/Bi₂O₃ composite with the formation of Bi-O-B bonding at the interfaces has been synthesized by solvothermal treatment at 165 °C for 4 h. The system works well as a sensor of flutamide, a nonsteroidal anti-androgen drug for the treatment of prostate cancer.^[56] The mixed bonding modifies the Bi₂O₃ bandgap because of the electron transfer at the interface, which increases to 5.7 eV for the h-BN/Bi₂O₃ composite. The difference in the work function between h-BN and Bi₂O₃, 5.81 and 4.7 eV, respectively, causes an upward Bi₂O₃ band bending and an electron transfer process while forming the heterojunction (Figure 5). Combined with a screen-printed carbon electrode (SPCE), the



Energy band diagram of Bi₂O₃/h-BN nanocomposite

Figure 5. Energy band diagram of the h-BN/Bi₂O₃ nanocomposite. Reproduced with permission.^[56] Copyright 2021, Elsevier.

electrochemical platform shows high selectivity for sensing flutamide in a linear range (0.04–87 μ M) with a 9.0 nM detection limit. The large exciton binding energy of the heterostructure favors the electron transfer process during the reduction of flutamide.

Du et al. have realized an h-BN/Bi₂MoO₆ heterojunction by the solvothermal synthesis in the presence of ultrathin h-BN sheets dispersed in an ethylene glycol solution of Bi(NO₃)₃ and Na₂MoO₄.^[57] The Bi₂MoO₆ particles grow and homogeneously distribute on the h-BN surface (Figure 6a); the system shows an effective photocatalytic degradation of tetracycline under visible light. The photoluminescence, photocurrent response and average lifetime suggest that h-BN plays the role of inhibiting the recombination of photogenerated electron–hole pairs (Figure 6b). The free radical trapping experiments have

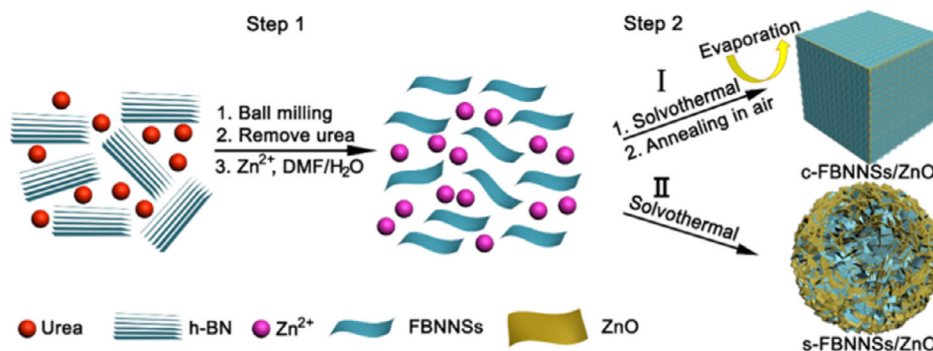


Figure 4. Synthetic procedure of a h-BN/ZnO heterostructure with 3D architecture. Reproduced with permission.^[53] Copyright 2019, American Chemical Society. Note: The letters “c-” and “s-” indicate the cubic and spherical morphologies, respectively; FBNNSs represent the h-BN nanosheets functionalized by -NH₂.

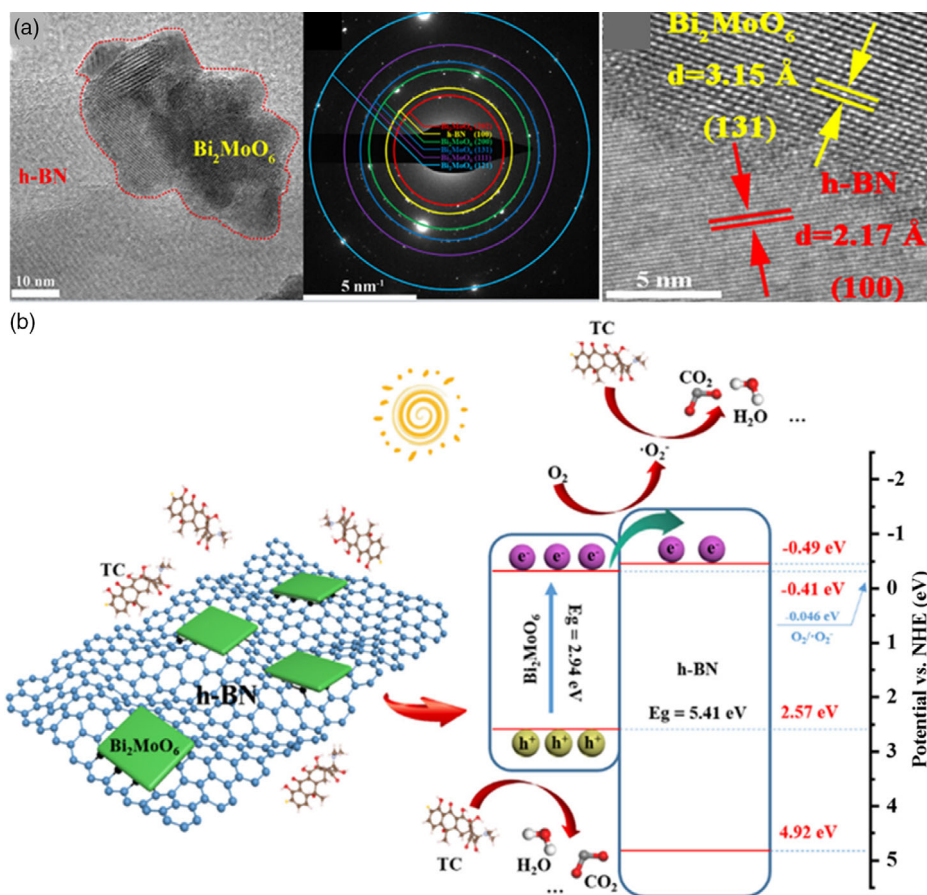


Figure 6. h-BN/Bi₂MoO₆ heterostructure. a) TEM images and b) the photocatalytic degradation mechanism of h-BN/Bi₂MoO₆ under visible-light irradiation. Reproduced with permission.^[57] Copyright 2021, Elsevier.

shown that h^+ and $O_2^{\cdot-}$ are the active species. Theoretical modeling by density functional theory (DFT) calculations has also indicated that the combination of h-BN and Bi₂MoO₆ effectively enhances the adsorption capability and lead to the activation and decomposition of tetracycline.

A solvothermal assembly has also been used for the preparation of h-BN-bismuth phosphate (BiPO₄) heterostructures.^[58] Given the poor dispersibility of h-BN, in this case, ionic liquid H₂PO₄ has been added into ethanol to mix Bi(NO₃)₃ and h-BN sheets. The resulted h-BN/BiPO₄ composite has shown an excellent capability to degrade the antibiotic enrofloxacin, which can be removed $\approx 91.5\%$ under UV irradiation for 2 h. Under illumination, the generated electrons can be excited from the valence band to the conduction band, and the holes will move to the valence band. The doping h-BN can lead to the suppressing recombination of the photogenerated carrier pairs (h^+ and e^-) in BiPO₄ and the generation of more $O_2^{\cdot-}$ and $\cdot OH$ radicals. This effect can further promote the photodegradation of enrofloxacin and weaken the photoluminescence of BiPO₄.^[58]

An h-BN/Bi₄O₅Br₂ heterojunction has been used for photocatalytic degradation of 4-*tert*-butylphenol.^[59] When the amount of h-BN is set at 1 wt%, the catalyst shows an optimized photoresponse which follows the first-order kinetics with a degradation rate of 0.02 min^{-1} . The theoretical simulations have revealed the photocatalytic mechanism (Figure 7); the heterostructure

can decrease the hybrid electron density of h-BN in the conduction band. Thus the electrons of h-BN will move to the Bi₄O₅Br₂ surface, inhibiting the recombination of electron-hole pairs.^[59]

Microwave is another method that allows preparing heterostructures via a homogeneous synthesis process. An h-BN/BiOCl composite has been synthesized via fast microwave-assisted heating.^[60] The reaction has been performed at 1000 W and 140 °C only for 1 h, which can effectively save production time and improve productivity. The composites possess a flower-like microsphere structure and can photocatalytically reduce Cr (VI) in an acidic solvent upon visible light irradiation.^[60] In an acidic medium, e.g., pH = 2, the h-BN/BiOCl composite can absorb H^+ , which not only allows the protonation but also accelerates the accumulation of Cr (VI), for example, Cr₂O₇²⁻ and HCrO₄⁻. In an alkaline environment, e.g., pH = 10, the absorptive capacity is severely restricted, and the generated sediment of Cr(OH)₃ would further block the optically active sites.

2.4. Boron Nitride–Noble Metal Heterostructures

Growing metal nanoparticles on the h-BN nanosheet surface is another route to form heterostructures. Gold, silver and copper are all feasible alternatives to add functional properties, Au

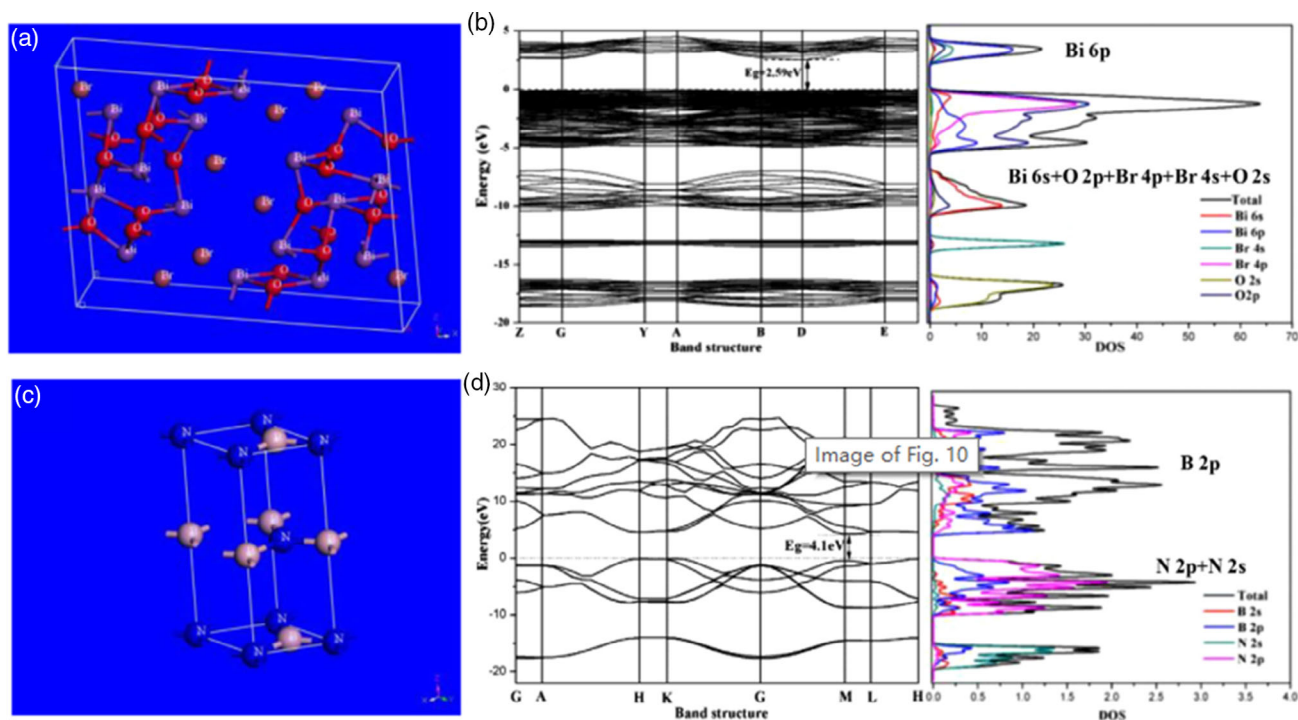


Figure 7. Crystal structures, simulated band structures, and states density of a) $\text{Bi}_4\text{O}_5\text{Br}_2$ and b) h-BN. Reproduced with permission.^[59] Copyright 2017, Elsevier.

supported by h-BN, for instance, improves the catalytic performances. Au nanoparticles have been heterogeneously grown on h-BN plates by reducing HAuCl_4 , showing a conversion and selectivity up to 100% in the hydrogenation of nitrobenzene.^[61] The h-BN sheets can refrain from oxygen activation, thereby endowing the catalytic hydrogenation of the nitrobenzene by the Au particles in the air. h-BN–Au heterostructures have also been tested for degrading lactose,^[62] and levofloxacin hydrochloride.^[63]

An h-BN/copper (Cu) composite has been successfully fabricated by solvothermal reduction of Cu^{2+} into Cu with the addition of a few-layer h-BN into the CuCl_2 precursor.^[64] Although the authors could not detect the formation of any chemical bonds between h-BN and the Cu matrix, the hetero-interface of the h-BN/Cu composite is well combined according to morphology analysis. Its thermal conductivity can achieve a maximum of $428 \text{ W m}^{-1} \text{ K}^{-1}$ when the content of h-BN is 6 wt%. The incorporation of h-BN reduces the thermal expansion coefficient of the composite.^[64]

BN nanomaterials doped with copper heteroatoms have been synthesized by the copolyolysis of Cu precursor (copper nitrate) and h-BN precursor (boric acid and melamine).^[65]

Doping the h-BN framework by Cu atoms produces an internal electric field due to the nonuniform electronic distribution with electropositive Cu and negative N sites. This field generates $\cdot\text{OH}$ radicals by promoting the reduction of H_2O_2 on N sites and the oxidation of H_2O on Cu sites. The h-BN/Cu composite efficiently degrades organic pollutants in water.^[65] The reduction of AgNO_3 upon microwave heating produce Ag nanoparticles on h-BN layers; the heterointerface is mainly connected via physical adsorption and electrostatic interaction.^[66] A composite

membrane, stable up to 85°C , can be obtained by filtration of h-BN/Ag dispersions. Its antibacterial activity and hydrophobicity make this composite a promising candidate for water disinfection.^[66] Ag nanoparticles can also nucleate on the h-BN surface through implanting Ag ions into hollow h-BN particles with a petal-like surface.^[67] The adjustment of ion energy in the 2–20 kV range allows tailoring the content of defective Ag crystallites and the fraction of the amorphous h-BN phase (see **Figure 8**). This has opened opportunities for producing hybrids for optoelectronic devices.^[67] In another case, h-BN/Ag heterostructure is successfully fabricated using one-pot pyrolysis of boron acid, urea, and AgNO_3 .^[68] The Ag modification can regulate the electronic structure of h-BN sheets, endowing the nanocomposites with enhanced adsorption performance towards tetracycline and RhB.

h-BN/platinum (Pt) nanohybrids have been prepared using a two-step synthesis^[69]: i) at first sonication with H_2O_2 induces the formation of hydroxyl to obtain hydrophilic h-BN sheets; ii) in the second step, Pt particles are formed on the h-BN surface by reducing K_2PtCl_4 upon the addition of ascorbic acid. Here, the chemical modification ensures uniform dispersion of Pt particles with a $\approx 8 \text{ nm}$ size, resulting in an enhancement of peroxidase mimetic activity. Furthermore, porous h-BN sheets can anchor more metal nanoparticles and activate a larger number of sites in the h-BN/Pt heterojunctions.^[70]

In a similar study, nickel (Ni) nanoclusters (ultrasmall size, $\approx 1.5 \text{ nm}$) have been immobilized on defect-rich h-BN sheets for improving hydrogen production from methanol.^[12] The bulk precursor has been preexfoliated by thermal treatment at 800°C followed by immersion in liquid nitrogen to obtain h-BN sheets

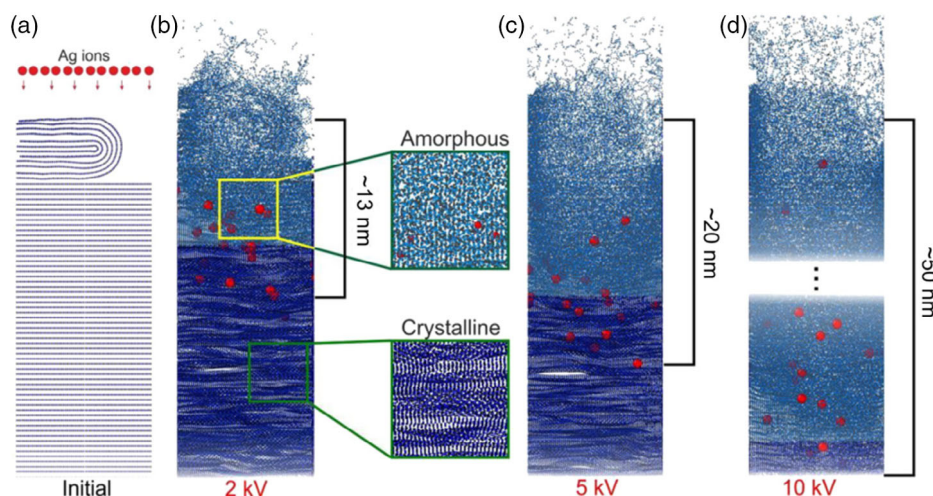


Figure 8. Schematic diagram of controlled h-BN/Ag heterostructure via Ag ion energy. Reproduced with permission.^[67] Copyright 2016, Elsevier.

with abundant oxygen vacancies. Sonication in a solution of tetrahydrofuran (THF) and lithium–naphthalenide produces the final exfoliation. The multistep exfoliation generates several defects, such as N-vacancy and O-doping. Then, the defective sites nucleate the Ni clusters using $\text{Ni}(\text{C}_5\text{H}_5)_2$ as the precursor.

Raman spectroscopy is a well-established nondestructive analytical tool, but its low sensitivity is considered a limitation to detect small amounts of analytes.^[71] For this reason, intensive research has been dedicated to developing specific systems that could increase the Raman scattering. Plasmonic structures, such as noble metal nanoparticles, have been largely employed for surface-enhanced Raman scattering (SERS).^[72] This route has also been explored in applying 2D h-BN for Raman sensing. h-BN–Au or Ag nanocomposites show significant Raman enhancements with respect to Au–silicon substrates or bare h-BNNSs.^[73–76] Cai et al. have prepared three SERS sensors by depositing Au nanoparticles on h-BNNS (atomically thin BN), bulk BN, and Si substrates; Rh 6G has been used as a testing molecule.^[73,74] The two BN–Au heterostructures show better Raman enhancements than the Au–Si substrate due to the affinity of aromatic molecules to the BN surface. The SERS signals from the h-BN monolayer are stronger than those from multilayer and bulk BN.^[73] The high thermal stability of h-BN gives an inherent advantage in reusing this type of sensor. The BN–Au sensor can be recycled after removing residual analytes by fast heating in the air (e.g., 400 °C for 5 min). Thermal treatment of the system gives better results than cleaning by solvent washing.^[74]

2.5. Other Boron Nitride–Metal Compound Heterostructures

Several h-BN heterostructures have been developed as dual cocatalysts for improving the photocatalytic response. The most general approach is using h-BN as support for growing oxide and metal nanoparticles. Some examples are (α - Fe_2O_3),^[77] cadmium sulfide (CdS),^[78] indium sulfide (In_2S_3),^[79] tin oxide (SnO_2),^[80] tin sulfide (SnS_2),^[81] zinc stannate (ZnSnO_3),^[82] tungsten trioxide (WO_3),^[83] antimony tungsten oxide (Sb_2WO_6),^[84] lead

tungstate (PbWO_4),^[85] zinc ferrite (ZnFe_2O_4),^[24] molybdenum oxide (MoO_2),^[86] copper oxide (Cu_2O),^[87] copper sulfide (CuS),^[88] silver bromide (AgBr),^[89] and silver carbonate (Ag_2CO_3).^[90] These particles have grown on h-BN with the main purpose to increase the charge transfer efficiency and reduce the recombination of hole–electron pairs.

In addition to photocatalysis, which is the most studied application by far, h-BN nanocomposites as electrocatalysts have also been designed.^[91–95] Patil et al. have reported a method to prepare an h-BN–manganese oxide (MnO_x) composite by adding h-BN during the reducing process of potassium permanganate (KMnO_4).^[91] h-BN supports the growth of MnO_x nanorods due to the seeding role played by the h-BN surface. Supported by ketjenblack carbon, the h-BN/ MnO_x cocatalyst shows an effective oxygen reduction capability, including a higher onset potential (0.9 V) and limiting kinetic current density (5.6 mA cm^{-2}).^[91]

Another example is the h-BN/ MnCe hetero-catalyst for selective catalytic reduction (SCR) technology.^[92] Aggregation of the catalyst, which reduces the conversion of nitrogen oxides into nontoxic gases, is the main drawback in SCR. A dispersion of the catalyst on proper support is a possible solution, and h-BN has been tested as a potential candidate. $\text{Co}(\text{NO}_3)_2$ has been used for etching exfoliated h-BN, and producing vacancy defects. MnO_x – CeO_x nanoparticles with an average size of 5 nm have been grown on the h-BN surface etched by immersing the flakes into the precursor solution of $\text{Mn}(\text{NO}_3)_2$ and $\text{Ce}(\text{NO}_3)_2$. The etched h-BN improves the dispersion of the catalyst and acts as a catalytically active site, thereby enhancing the SCR performance.^[92]

Figure 9 shows the scheme of a sonochemical method used to prepare 2D layered BN–titanium carbide (TiC) heterojunctions by ultrasonating their bulk counterparts together.^[25] The obtained h-BN/TiC composite is an electrocatalyst that exhibits an improved sensing response to sulfadiazine due to its larger number of active sites, higher conductivity, and enhanced surface area.

Semiconductor colloidal quantum dots (QDs) are efficient light-conversion phosphors in the photonics industry.^[96] However, the thermal quenching has severely hindered the applications of QDs-devices, e.g., white light-emitting diodes

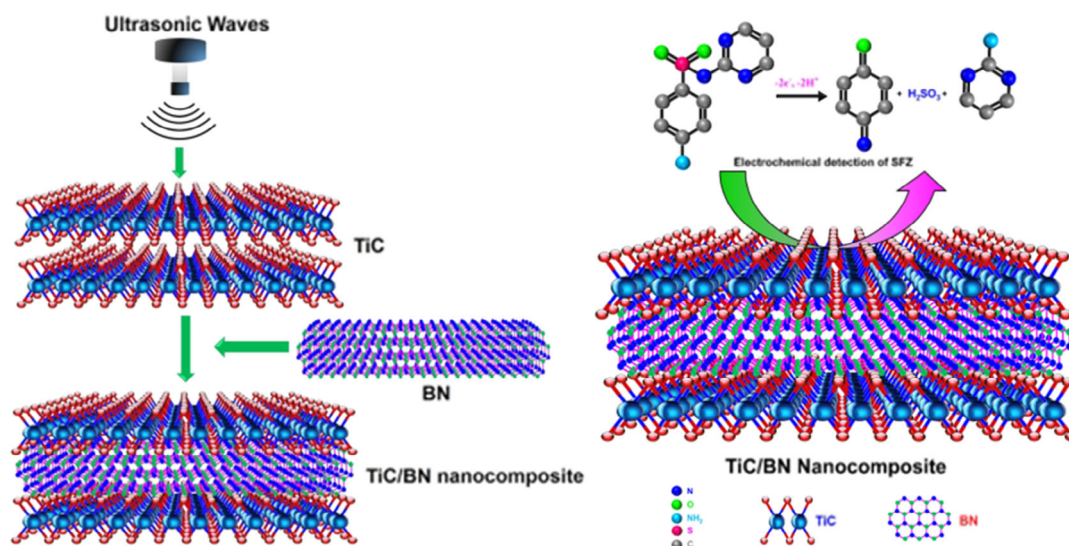


Figure 9. Schematic illustration for the synthesis of a h-BN/TiC heterostructure and electrochemical mechanism for the detection for sulfadiazine. Reproduced with permission.^[25] Copyright 2020, American Chemical Society.

(WLEDs), because of the low thermal conductivity. The combination with h-BN, which has good thermal conductivity, has the advantage of better heat dissipation of the “heat sources” represented by QDs. The better heat dissipation efficiency extends the device service life. An example (**Figure 10a**) is the h-BN/QDs heterojunction obtained by bonding, through electrostatic interaction, CdSe/ZnS core-shell QDs on the h-BN platelets surface.

The system is then embedded into a silicone matrix as a phosphor in WLEDs.^[97] **Figure 10b** shows the electroluminescence spectra of the fabricated WLEDs based on QDs and h-BN/QDs, respectively. Incorporating h-BN causes negligible influence on the devices’ optical performances and even increases the luminous efficiency (111.7 vs 108.5 lm W⁻¹). The simulated temperature fields of the WLEDs in **Figure 10c**

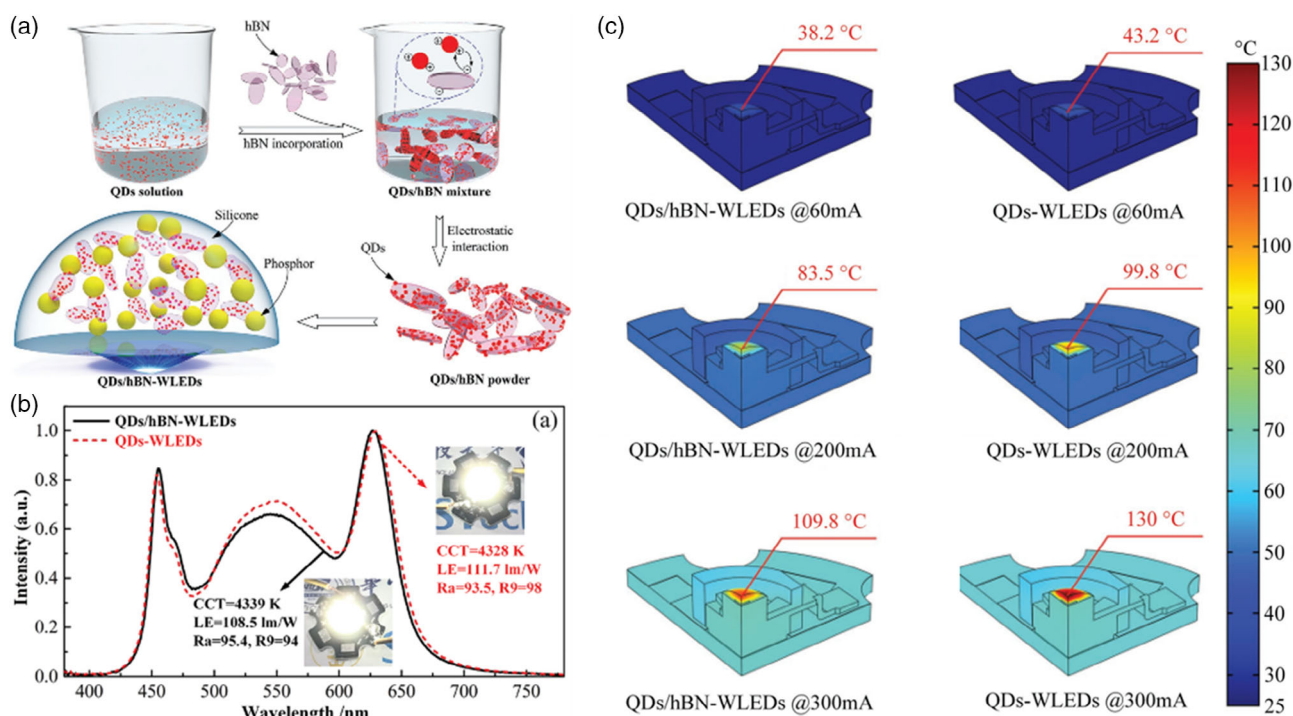


Figure 10. a) Schematic illustration for synthesizing h-BN/QDs composites and their application in WLEDs. b) Electroluminescence spectra of the fabricated WLEDs based on QDs and h-BN/QDs under 20 mA driving current. c) The measured temperature fields of the two WLEDs at different currents. Reproduced with permission.^[97] Copyright 2018, Wiley-VCH.

prove that the h-BN/QDs heterostructure effectively reduces the working temperature. Other studies have targeted perovskite QDs onto h-BN sheets for WLEDs, showing improved lighting stability^[26]; the system can be used as a fluorescent sensor to detect pollutant antibiotics, e.g., tetracycline.^[98]

3. Boron Nitride–Nonmetallic Heterostructures

3.1. Boron Nitride–Graphene Heterostructures

Graphene is the structural analogous of BN, and both graphene and reduced graphene oxide (rGO) have shown to form heterojunctions with h-BN by a solvothermal or hydrothermal route followed by an annealing treatment in a nitrogen atmosphere.^[99,100] h-BN-graphene heterostructures are rising a growing interest.^[101–103]

Huang et al. have studied the effects of h-BN, combined with GO or rGO, on the thermal conductivity of an epoxy resin matrix.^[104,105] h-BN nanosheets have been functionalized with –OH groups by ultrasonication, then modified by 3-aminopropyltriethoxysilane (APTES). The APTES as coupling agent ensures a good encapsulation of h-BN by GO and rGO to form a hybrid heterostructure. When incorporating BN-GO^[104] or BN-rGO^[105] hybrids into an epoxy matrix, the thermal conductivity of the epoxy composites can reach 2.23 or 3.45 W m⁻¹ K⁻¹ respectively, whereas the value is only 0.24 W m⁻¹ K⁻¹ for a pure epoxy resin. Herein, the GO or rGO can serve as effective bridges for h-BN and markedly reduce the interfacial thermal resistance between h-BN and epoxy resin. Moreover, the addition of GO/rGO and APTES can also prevent the agglomeration of h-BN and integrate the thermal-conductive pathway of the resulted polymer composites. In another study, Yang et al. report that the incorporation of h-BN/rGO hybrid produces a ten times enhancement of the thermal conductivity of polyethylene glycol (M_n = 10 000).^[106]

Guo et al. have proposed a sequential strategy to fabricate a micro-sandwich structure by alternately stacking insulating h-BN sheets and conductive rGO layers.^[107] The resulting h-BN/rGO sandwich hybrid is an excellent dielectric and has high thermal conductivity, with potential applications in capacitive energy storage. The authors explain that the phonon transport at the aligning h-BN/rGO heterointerfaces is more efficient than in the case of randomly mixed sheets (see Figure 11a).^[107] If graphene is substituted by h-BN/graphene as the interlayer of lithium-sulfur batteries, the capacity improves from 382 to 560 mAh g⁻¹.^[108]

Engineering 2D layered h-BN/graphene heterojunctions is an important strategy to design advanced metal-free nanocatalysts, which can avoid the poor charge mobility of semiconductor catalysts.^[109] Zhang et al. have developed atomic-scale h-BN/graphene Mott–Schottky heterojunctions as metal-free photocatalysts for artificial photosynthesis.^[110] The heterostructure has been prepared by direct copolymerization of glucose, boric acid, and urea in the presence of a controlled amount of graphene and h-BN layers (see Figure 11b). The interfacial Schottky barrier promotes the separation of the photogenerated charge carriers and direct activation of the substrate and oxygen molecules. The increased lifetime of the photogenerated electrons enhances the photocatalytic activation of oxygen gas for oxidative coupling of amines into imines.^[110]

An interesting synthesis route is preparing hybridized atomic layers of h-BN and graphene to obtain boron–carbon–nitrogen (BCN) heterolayers, where fractions of h-BN domains can be substituted with graphene regions or vice versa. The optical gaps and electronic properties of the hybridized layers will have intermediate properties with respect to isolated graphene or h-BN.^[111] Graphene islands in a planar h-BN matrix have been observed from BCN layer^[112]; h-BN islands in a graphene matrix have been fabricated via CVD method.^[113]

These BCN heterojunctions have envisaged the possible development of bandgap-engineered materials in electronics and

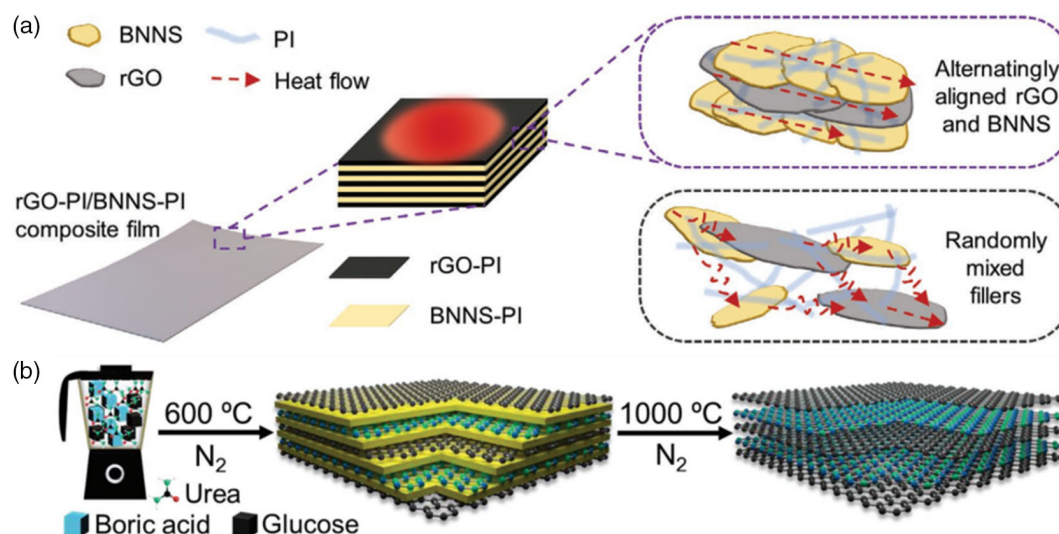


Figure 11. a) Schematics diagram for high thermal conductivity from h-BN/rGO sandwich composite. Reproduced with permission.^[107] Copyright 2020, Wiley-VCH. b) Schematics synthetic paths for h-BN/graphene Mott–Schottky heterojunctions. Reproduced under the terms of the Creative Commons CC-BY license.^[110] Copyright 2018, The Authors. Published by Wiley-VCH.

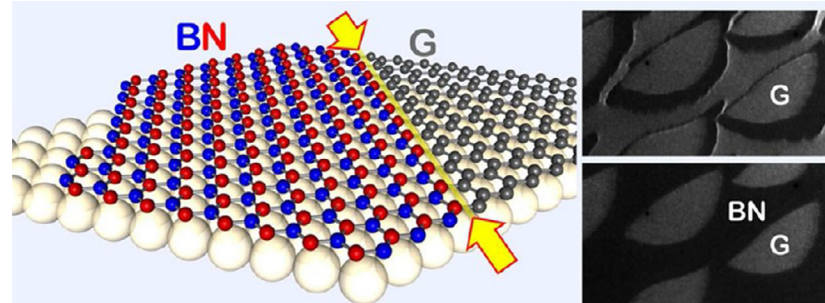


Figure 12. Interface in a monolayer graphene–h-BN heterostructure. Reproduced with permission.^[115] Copyright 2012, American Chemical Society.

optics. In an example reported by Huang et al., a ternary BCN component has been prepared by heating boron oxide, urea and glucose at 1250 °C for 5 h.^[114] The theoretical simulation shows that the doped carbon can reduce the band gap of h-BN from 4.56 to 2.00 eV (2.08 eV, experimental value), enabling an excellent visible light photocatalytic response for H₂ generation.

Another exciting option is the preparation of h-BN–graphene interfaces in low dimensions, the two materials integrated in a single 2D layer appear separated by a line boundary (**Figure 12**). Taking advantage of the graphene–h-BN isostructure and nearly lattice-matching, heterojunctions have been formed on a ruthenium substrate using a sequential chemical vapor deposition process. High-temperature growth gives intermixing near the interface, similar to interfacial alloying in conventional heterostructures.^[115]

3.2. Boron Nitride–Carbonitride Heterostructures

Graphite carbon nitride (g-C₃N₄) is one of the most promising 2D materials beyond graphene and has been largely applied in photocatalysis, CO₂ reduction, water splitting, etc.^[116] Both h-BN and C₃N₄ are structurally analogous to graphene with a π - π conjugated structure, enabling a tight binding interface when fabricating a heterojunction. Xu and co-workers have produced h-BN/C₃N₄ nanocomposites with a B=C bonding by using a glazed ultrasonic stripping of h-BN sheets directly onto the surface of an analogously stripped g-C₃N₄ sheet.^[117] The heterojunction creates an intimate interface and activates an efficient interfacial charge transfer, improving the charge separation and photocatalytic response.

A binary h-BN/CN composite with a type-II p–n heterojunction has been prepared by calcining n-type h-BN and p-type boron-doped CN. The composite shows an effective degradation toward tetracycline hydrochloride upon sunlight irradiation.^[118] The measured conduction and valence bands of B-doped CN are –2.20 and 0.30 eV, lower than –0.20 and 5.20 eV of h-BN. However, the band bending cannot contribute to the generation of superoxide and hydroxyl radicals, in disagreement with the requirement of a double charge transfer path (see **Figure 13a**). A solid-state Z-scheme mechanism has been suggested to explain the effective photocatalytic response.^[118] Under excitation by sunlight (**Figure 13b**), the interfaces can act as intermediates, which react with the electrons and indirectly cause their

transmission from the conduction band of h-BN to the valence band of CN.

He et al. have directly used urea to grow by annealing layered carbonitride (CN) on porous h-BN nanosheets to fabricate h-BN/CN composites.^[119] The h-BN/CN band gap shifts from 3.84 to 2.67 eV when the CN is loaded from 0 (pure BN) to 100% (pure CN), enhancing its light absorption efficiency. In this heterojunction, the electrons photogenerated in CN can be transferred to the h-BN phase and the holes from h-BN to the CN surface, finally demonstrating an enhanced photocatalytic H₂ production.^[119] Another h-BN/CN heterostructure has been obtained by calcination of exfoliated h-BN and CN sheets.^[120] The shift of XPS binding energy confirms the interfacial interaction and the transfer of electrons from CN to h-BN. When the loading of h-BN is 1.5 wt%, the composite shows the maximum photocatalytic H₂ generation, as well as an effective degradation of tetracycline hydrochloride.^[120]

A 2D/0D h-BN-C₃N₄ heterostructure can be produced by embedding g-C₃N₄ QDs into 2D h-BN materials, via calcination of melamine and h-BN mixtures.^[121] The morphological analysis of the composite has shown that the g-C₃N₄ dots can be well entrenched on the h-BN surface. The BET data suggest that the heterostructure has an enlarged surface area (80.2 m² g^{–1}) in comparison to the bulk g-C₃N₄ (14.3 m² g^{–1}), which can provide more active sites. The –OH groups of h-BN are also contributing to the electron transfer in the photocatalysis.

4. Boron Nitride van der Waals Heterostructures

van der Waals heterostructures are at the center of an increasing interest, particularly, in the field of electronics and optoelectronics.^[18] Heterostructures made by designing a specific layer by layer sequence are indicated as van der Waals heterostructures.^[122] h-BN layers have also been used to build such heterojunctions.

This type of atomically thin heterostructures show unprecedented functions due to the combined effects created by the controlled overlapping of different 2D layers.^[30] Importantly, there are no restrictions on lattice matching and processing compatibility, which makes possible fabricating a wide range of different heterostructures.^[123] Unlike heterostructures where defects govern the functional properties, such as BN for photonic applications, it is important in the case of van der Waals materials that the 2D layers of h-BN are possibly free from defects.

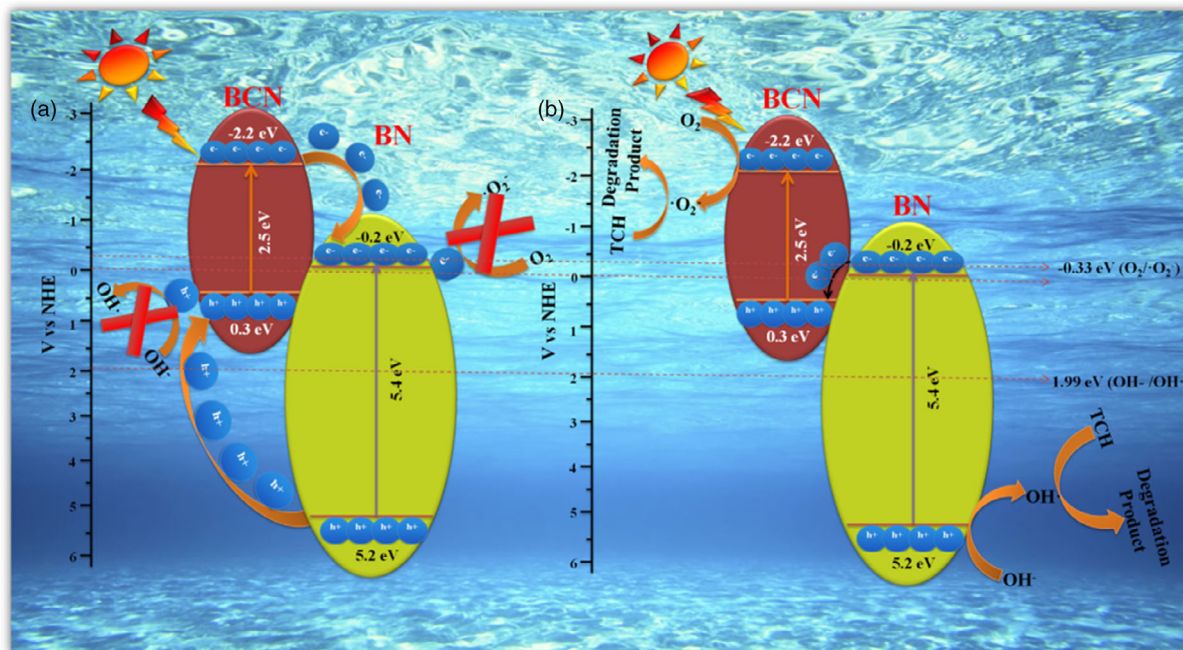


Figure 13. Schematic representations of a h-BN/CN photocatalyst. a) double charge transfer path, and b) Z-scheme mechanism. Reproduced with permission.^[118] Copyright 2020, Elsevier.

Currently, chemical vapor deposition (CVD) is the main technique to produce high-quality van der Waals heterojunctions on a large scale. Considering that the direct growth of h-BN on graphene usually damages graphene itself,^[124] the most common route is to synthesize graphene on h-BN surface via CVD. For example, h-BN can be first grown on a copper substrate using ammonia borane as source; nichel atoms from the decomposition of nickelocene at 850 °C are employed to decrease the energy barrier for growing graphene. In this way, vertically stacked graphene/h-BN heterostructures have been fabricated (Figure 14a).^[125] Interestingly, the graphene possesses a relative rotation angle regarding the h-BN resulting in a moiré pattern with periodicity of 8 nm.

In alternative to stacking different 2D crystals on top of each other, Zhang et al. have designed a cosegregation method to produce wafer-scale heterostructures via simultaneous growth of graphene and BN.^[126] In this process, a sandwiched substrate is at first fabricated on a Ni film, using a solid BN source, and a C-doped Ni layer (see Figure 14b); an annealing treatment can lead to the final hybrid h-BN–graphene on Ni surface via diffusion of B and N atoms to the surface where they nucleate and grow to form an h-BN layer between graphene and Ni surface.

Apart from graphene, transition metal dichalcogenides (TMDs) are other layered materials that create functional van der Waals heterostructures with h-BN. Similarly to graphene, the main fabrication route is also a direct growth of TMD layer

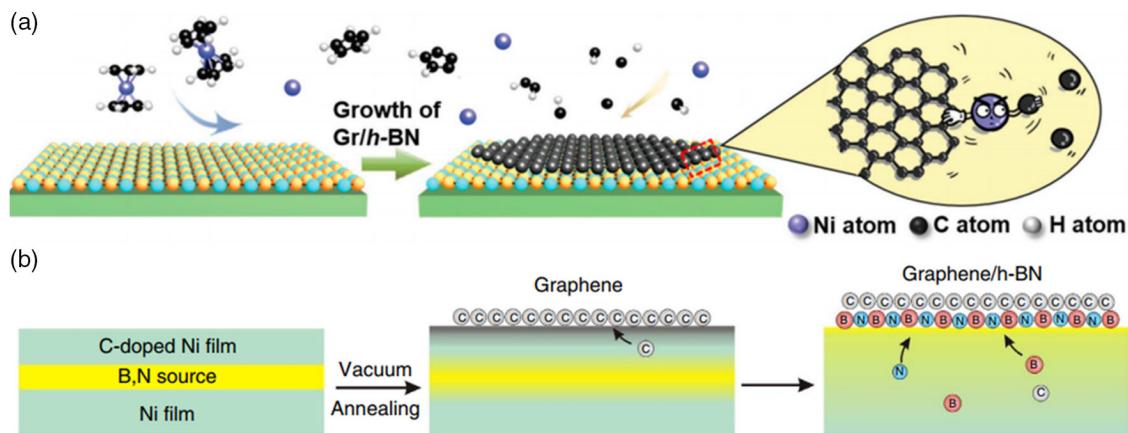


Figure 14. Schematic preparation of h-BN-graphene van der Waals heterostructures via a) direct growth of h-BN on graphene and b) cosegregation method. a) Reproduced with permission.^[125] Copyright 2017, Wiley-VCH. b) Reproduced with permission.^[126] Copyright 2015, Nature Publishing Group.

on h-BN supported by a metal foil.^[30] Zhang and co-workers have used a CVD technique to grow MoS₂ from MoO₃ and S precursors on a h-BN/Au substrate.^[127] The h-BN layer can largely diminish the interactions between the MoS₂ layer and Au foil, with luminescence quenching from TMDs. Meanwhile, the weak interfacial interactions allow transferring the BN-MoS₂ heterostructure from the foil to arbitrary substrates.^[127] This feature allows the reuse of the Au foil and enables the fabrication of electronic devices based on h-BN in van der Waals heterostructures.

The construction of multiple heterostructures can greatly enrich the functional properties of h-BN van der Waals systems. Memory devices based on van der Waals heterostructures have been fabricated via an assembly of conductive/insulative/semiconductive atomically thin 2D layers in a layer-by-layer stacking way, consequently resulting in an ideal combination of heterostructure and tunnelling.^[128] Very recently, two types of ternary van der Waals heterostructures, InSe/h-BN/graphene and MoS₂/h-BN/graphene have been successfully prepared and applied in flash memory devices.^[129,130] Both the heterostructured devices can achieve an ultrahigh-speed programming/erasing operation in the nanosecond time scale (20 ns), while the retention time can reach ten years.

5. Challenges and Opportunities for the Future

The fabrication of heterostructures–heterojunctions from 2D h-BN is an emerging field of research, and several possible applications have been demonstrated. However, the present review has shown how this topic has not yet been explored systematically, and several scattered studies have been devoted mainly to improving some of the properties in devices, especially in photocatalysis. The main drawback is that basic research in h-BN is still lagging and a clear correspondence between defects and properties has to be experimentally assessed. Managing defects in h-BN is the key to the actual exploitation of h-BN properties. On the contrary, van der Waals heterostructures generally require high-quality and possibly defect-free h-BN layers to take advantage of the high thermal conductivity and electrical insulation.

Another issue is related to the technology of h-BN fabrication; it has still to be fully assessed in terms of reproducibility and control. The fabrication techniques do not allow, up to now, to obtain h-BN nanosheets with a very controlled number of layers. The dimensions are also defined in terms of average size. This suggests that applications, where strict control of the properties is not required, should be more feasible.

One of the most explored applications for h-BN 2D materials is photocatalysis. It has demonstrated that the h-BN based heterostructures increase, in general, the charge separation and improve the performances. However, the role of the interface has still to be clarified; the presence of mixed bonding seems to be an important factor, but interphase bonding needs to be explored much more in detail. Band gap and defects engineering of the h-BN heterojunctions need to be performed in a systematic way to achieve a rationale design of the heterostructure.

In general, the fabrication of heterostructures can follow two strategies, improving known properties, such as the photocatalytic response, or combining the properties of the different

materials. Multicomponent heterostructures of increasing complexity can be designed to add different functions, and this route for h-BN is still largely unexplored. One of the most attractive properties of h-BN is the high thermal conductivity combined with electrical isolation; this should allow, as demonstrated in some works, to build heterostructures which could play multiple functions and dissipate heat during operation.

h-BN plays also an important role in the fabrication of van der Waals heterostructures. This is one of the most promising fields of applications for 2D BN where the high thermal conductive and electric insulation properties can be exploited to build stacking multilayered heterostructures. In addition to heterostructures, homostructures with different h-BN stacking are also an option to explore. Very recently, Woods et al. have observed a ferroelectric effect from twisted h-BN bilayers, where the triangular domains are the regions of AB and BA alternately stacking.^[131] h-BN homostructures by nanomechanically rotating and locking stacks of h-BN bulk crystals have been also fabricated, and the observation of second harmonic generation can be modulated over 50 times.^[132] The findings from h-BN homojunctions are opening up more possibilities for heterostructure design. The challenges are all there together with many opportunities.

Acknowledgements

The authors acknowledge Banco di Sardegna, Project MADMAT. Fondi liberi di Ateneo 2019–2020.

Open Access Funding provided by Università degli Studi di Sassari within the CRUI-CARE Agreement.

Conflict of Interest

The authors declare no conflict of interest.

Keywords

boron nitride, heterojunctions, heterostructures, 2D materials

Received: May 17, 2021

Revised: July 20, 2021

Published online:

- [1] M. Yankowitz, Q. Ma, P. Jarillo Herrero, B. J. LeRoy, *Nat. Rev. Phys.* **2019**, *1*, 112.
- [2] C. Yu, J. Zhang, W. Tian, X. Fan, Y. Yao, *RSC Adv.* **2018**, *8*, 21948.
- [3] L. H. Li, J. Cervenka, K. Watanabe, T. Taniguchi, Y. Chen, *ACS Nano* **2014**, *8*, 1457.
- [4] Q. Cai, D. Scullion, W. Gan, A. Falin, S. Zhang, K. Watanabe, T. Taniguchi, Y. Chen, E. J. G. Santos, L. H. Li, *Sci. Adv.* **2019**, *5*, eaav0129.
- [5] K. Watanabe, T. Taniguchi, H. Kanda, *Nat. Mater.* **2004**, *3*, 404.
- [6] J. D. Caldwell, I. Aharonovich, G. Cassabois, J. H. Edgar, B. Gil, D. N. Basov, *Nat. Rev. Mater.* **2019**, *4*, 552.
- [7] J. Ren, L. Stagi, P. Innocenzi, *J. Mater. Sci.* **2021**, *56*, 4053.
- [8] J. Ren, L. Stagi, C. M. Carbonaro, L. Malfatti, M. F. Casula, P. C. Ricci, A. E. Del Rio Castillo, F. Bonaccorso, L. Calvillo, G. Granozzi, P. Innocenzi, *2D Mater.* **2020**, *7*, 045023.
- [9] L. Stagi, J. Ren, P. Innocenzi, *Materials* **2019**, *12*, 3905.

- [10] B. Mortazavi, L. F. C. Pereira, J.-W. Jiang, T. Rabczuk, *Sci. Rep.* **2015**, *5*, 13228.
- [11] Z. Wang, P. Priego, M. J. Meziani, K. Wirth, S. Bhattacharya, A. Rao, P. Wang, Y.-P. Sun, *Nanoscale Adv.* **2020**, *2*, 2507.
- [12] Z. Zhang, J. Su, A. S. Matias, M. Gordon, Y.-S. Liu, J. Guo, C. Song, C. Dun, D. Prendergast, G. A. Somorjai, J. J. Urban, *Proc. Natl. Acad. Sci.* **2020**, *117*, 29442.
- [13] J. H. Los, J. M. H. Kroes, K. Albe, R. M. Gordillo, M. I. Katsnelson, A. Fasolino, *Phys. Rev. B* **2017**, *96*, 184108.
- [14] J. Ren, L. Malfatti, S. Enzo, C. M. Carbonaro, L. Calvillo, G. Granozzi, P. Innocenzi, *J. Colloid Interface Sci.* **2020**, *560*, 398.
- [15] A. Reserbat Plantey, I. Epstein, I. Torre, A. T. Costa, P. A. D. Gonçalves, N. A. Mortensen, M. Polini, J. C. W. Song, N. M. R. Peres, F. H. L. Koppens, *ACS Photonics* **2021**, *8*, 85.
- [16] C. Zhou, C. Lai, C. Zhang, G. Zeng, D. Huang, M. Cheng, L. Hu, W. Xiong, M. Chen, J. Wang, *Appl. Catal. B Environ.* **2018**, *238*, 6.
- [17] S. Yu, X. Wang, H. Pang, R. Zhang, W. Song, D. Fu, T. Hayat, X. Wang, *Chem. Eng. J.* **2018**, *333*, 343.
- [18] K. K. Kim, H. S. Lee, Y. H. Lee, *Chem. Soc. Rev.* **2018**, *47*, 6342.
- [19] J. Tan, S. Li, B. Liu, H. Cheng, *Small Struct.* **2021**, *2*, 2000093.
- [20] N. Wang, G. Yang, H. Wang, R. Sun, C. P. Wong, *Front. Chem.* **2018**, *6*, 440.
- [21] X. Li, J. Zhang, S. Zhang, S. Xu, X. Wu, J. Chang, Z. He, *J. Alloys Compd.* **2021**, *864*, 158153.
- [22] Y. Sheng, J. Yang, F. Wang, L. Liu, H. Liu, C. Yan, Z. Guo, *Appl. Surf. Sci.* **2019**, *465*, 154.
- [23] H. He, W. Wang, C. Xu, S. Yang, C. Sun, X. Wang, Y. Yao, N. Mi, W. Xiang, S. Li, *Sci. Total Environ.* **2020**, *730*, 139100.
- [24] E. Erusappan, S. Thiripuranthagan, M. Durai, S. Kumaravel, T. Vembuli, *New J. Chem.* **2020**, *44*, 7758.
- [25] T. Kokulnathan, E. Ashok Kumar, T. J. Wang, *ACS Sustainable Chem. Eng.* **2020**, *8*, 12471.
- [26] Y. Li, L. Dong, N. Chen, Z. Guo, Y. Lv, J. Zheng, C. Chen, *ACS Appl. Mater. Interfaces* **2019**, *11*, 8242.
- [27] M. L. Yola, N. Atar, *Mater. Sci. Eng. C* **2019**, *96*, 669.
- [28] S. Cheng, T. Ye, H. Mao, Y. Wu, W. Jiang, C. Ban, Y. Yin, J. Liu, F. Xiu, W. Huang, *Nanoscale* **2020**, *12*, 524.
- [29] X. Hou, Z. Zhang, X. Wei, Y. Qin, G. Song, L. Li, M. Li, W. Dai, S. Zhao, C. T. Lin, N. Jiang, J. Yu, *ACS Appl. Nano Mater.* **2021**, *4*, 2136.
- [30] J. Zhang, B. Tan, X. Zhang, F. Gao, Y. Hu, L. Wang, X. Duan, Z. Yang, P. Hu, *Adv. Mater.* **2021**, *33*, 2000769.
- [31] C. Peng, H. Xing, X. Fan, Y. Xue, J. Li, E. Wang, *Anal. Chem.* **2019**, *91*, 5762.
- [32] A. Meng, L. Zhang, B. Cheng, J. Yu, *Adv. Mater.* **2019**, *31*, 1807660.
- [33] D. Liu, M. Zhang, W. Xie, L. Sun, Y. Chen, W. Lei, *Appl. Catal. B Environ.* **2017**, *207*, 72.
- [34] A. U. Ahmad, A. Abbas, S. Ali, M. Fakhar e-alam, Z. Farooq, Q. Abbas, M. Ahmad, A. Farid, H. M. U. Arshad, M. Javid, *Ceram. Int.* **2021**, *47*, 10089.
- [35] J. Ren, L. Stagi, L. Malfatti, S. Garroni, S. Enzo, P. Innocenzi, *Langmuir* **2021**, *37*, 5348.
- [36] G.-J. Lai, L.-M. Lyu, Y.-S. Huang, G.-C. Lee, M.-P. Lu, T.-P. Perng, M.-Y. Lu, L.-J. Chen, *Nano Energy* **2021**, *81*, 105608.
- [37] W.-Z. Xiao, L. Xu, Q.-Y. Rong, X.-Y. Dai, C.-P. Cheng, L.-L. Wang, *Appl. Surf. Sci.* **2020**, *504*, 144425.
- [38] W. Lei, D. Portehault, D. Liu, S. Qin, Y. Chen, *Nat. Commun.* **2013**, *4*, 1777.
- [39] Z. Zheng, M. Cox, B. Li, *J. Mater. Sci.* **2018**, *53*, 66.
- [40] L. H. Li, Y. Chen, B.-M. Cheng, M.-Y. Lin, S.-L. Chou, Y.-C. Peng, *Appl. Phys. Lett.* **2012**, *100*, 261108.
- [41] X. Fu, Y. Hu, Y. Yang, W. Liu, S. Chen, *J. Hazard. Mater.* **2013**, *244*, 102.
- [42] G. Ni, Y. Li, S. Wang, Q. Li, *Mater. Lett.* **2021**, *288*, 129385.
- [43] B. Singh, G. Kaur, P. Singh, K. Singh, J. Sharma, M. Kumar, R. Bala, R. Meena, S. K. Sharma, A. Kumar, *New J. Chem.* **2017**, *41*, 11640.
- [44] L. Malfatti, P. Falcaro, A. Pinna, B. Lasio, M. F. Casula, D. Locher, A. Falqui, B. Marmiroli, H. Amenitsch, R. Sanna, A. Mariani, P. Innocenzi, *ACS Appl. Mater. Interfaces* **2014**, *6*, 795.
- [45] Z. He, C. Kim, T. H. Jeon, W. Choi, *Appl. Catal. B Environ.* **2018**, *237*, 772.
- [46] C. Y. Su, H. Z. Tang, K. Chu, C. K. Lin, *Ceram. Int.* **2014**, *40*, 6903.
- [47] Z. Huang, W. Zhao, *Prog. Org. Coat.* **2020**, *148*, 105881.
- [48] M. Shanmugam, R. Jacobs-Gedrim, C. Durcan, B. Yu, *Nanoscale* **2013**, *5*, 11275.
- [49] M. Nasr, R. Viter, C. Eid, R. Habchi, P. Miele, M. Bechelany, *New J. Chem.* **2017**, *41*, 81.
- [50] L. Lin, W. Jiang, M. Nasr, M. Bechelany, P. Miele, H. Wang, P. Xu, *Photochem. Photobiol. Sci.* **2019**, *18*, 2921.
- [51] B. Hussain, M. Y. A. Raja, N. Lu, I. Ferguson, *2013 High Capacity Optical Networks and Emerging/Enabling Technologies*, IEEE, Piscataway, NY **2013**.
- [52] X. Fu, Y. Hu, T. Zhang, S. Chen, *Appl. Surf. Sci.* **2013**, *280*, 828.
- [53] C. Yang, D. Liu, Y. Chen, C. Chen, J. Wang, Y. Fan, S. Huang, W. Lei, *ACS Appl. Mater. Interfaces* **2019**, *11*, 10276.
- [54] M. Özgür, S. Pat, R. Mohammadigharehbagh, U. Demirkol, N. Akkurt, A. Olkun, Ş. Korkmaz, *J. Mater. Sci. Mater. Electron.* **2020**, *31*, 6948.
- [55] S. Yu, L. Zhang, L. Zhu, Y. Gao, G. Fan, D. Han, G. Chen, W. Zhao, *Coord. Chem. Rev.* **2019**, *393*, 9.
- [56] T. Kokulnathan, R. Vishnuraj, T.-J. Wang, E. A. Kumar, B. Pullithadathil, *Ecotoxicol. Environ. Saf.* **2021**, *207*, 111276.
- [57] Z. Du, L. Feng, Z. Guo, T. Yan, Q. Hu, J. Lin, Y. Huang, C. Tang, Y. Fang, *J. Colloid Interface Sci.* **2021**, *589*, 545.
- [58] Z. Chen, X. Chen, J. Di, Y. Liu, S. Yin, J. Xia, H. Li, *J. Colloid Interface Sci.* **2017**, *492*, 51.
- [59] S. Ding, D. Mao, S. Yang, F. Wang, L. Meng, M. Han, H. He, C. Sun, B. Xu, *Appl. Catal. B Environ.* **2017**, *210*, 386.
- [60] H. Xu, Z. Wu, M. Ding, X. Gao, *Mater. Des.* **2017**, *114*, 129.
- [61] Q. Liu, Y. Xu, X. Qiu, C. Huang, M. Liu, *J. Catal.* **2019**, *370*, 55.
- [62] N. Meyer, C. Renders, R. Lanckman, M. Devillers, S. Hermans, *Appl. Catal. A* **2015**, *504*, 549.
- [63] Y. He, N. Xu, L. B. Junior, X. Hao, B. Yao, Q. Yang, D. Liu, Z. Ma, *Appl. Surf. Sci.* **2020**, *520*, 146336.
- [64] D. Wan, X. Wu, W. Zhang, K. Peng, *Mater. Res. Bull.* **2019**, *120*, 110606.
- [65] L. Li, C. Hu, L. Zhang, G. Yu, L. Lyu, F. Li, N. Jiang, *J. Mater. Chem. A* **2019**, *7*, 6946.
- [66] G. Gao, A. Mathkar, E. P. Martins, D. S. Galvão, D. Gao, P. A. D. S. Autreto, C. Sun, L. Cai, P. M. Ajayan, *J. Mater. Chem. A* **2014**, *2*, 3148.
- [67] K. L. Firestein, D. G. Kvashnin, A. N. Shevko, I. V. Sukhorukova, A. M. Kovalskii, A. T. Matveev, O. I. Lebedev, P. B. Sorokin, D. Golberg, D. V. Shtansky, *Mater. Des.* **2016**, *98*, 167.
- [68] J. Pang, Y. Chao, H. Chang, H. Li, J. Xiong, Q. Zhang, G. Chen, J. Qian, W. Zhu, H. Li, *ACS Sustainable Chem. Eng.* **2018**, *6*, 4948.
- [69] M. N. Ivanova, E. D. Grayfer, E. E. Plotnikova, L. S. Kibis, G. Darabdhara, P. K. Boruah, M. R. Das, V. E. Fedorov, *ACS Appl. Mater. Interfaces* **2019**, *11*, 22102.
- [70] Q. Li, L. Li, X. Yu, X. Wu, Z. Xie, X. Wang, Z. Lu, X. Zhang, Y. Huang, X. Yang, *Chem. Eng. J.* **2020**, *399*, 125827.
- [71] P. Innocenzi, L. Malfatti, *TrAC Trends Anal. Chem.* **2019**, *114*, 233.
- [72] A. Campion, P. Kambhampati, *Chem. Soc. Rev.* **1998**, *27*, 241.
- [73] Q. Cai, S. Mateti, K. Watanabe, T. Taniguchi, S. Huang, Y. Chen, L. H. Li, *ACS Appl. Mater. Interfaces* **2016**, *8*, 15630.

- [74] Q. Cai, L. H. Li, Y. Yu, Y. Liu, S. Huang, Y. Chen, K. Watanabe, T. Taniguchi, *Phys. Chem. Chem. Phys.* **2015**, *17*, 7761.
- [75] A. U. Ahmad, Q. Abbas, S. Ali, M. Fakhar-e-alam, Z. Farooq, A. Farid, A. Abbas, M. Javid, A. Muhammad Afzal, H. M. Umair Arshad, M. Iqbal, *Ceram. Int.* **2021**, *47*, 6528.
- [76] Q. Cai, S. Mateti, W. Yang, R. Jones, K. Watanabe, T. Taniguchi, S. Huang, Y. Chen, L. H. Li, *Angew. Chem. Int. Ed.* **2016**, *55*, 8405.
- [77] M. R. Shenoy, S. Ayyasamy, V. Bhojan, R. Swaminathan, N. Raju, P. S. Kumar, M. Sasikumar, G. Kadarkarai, S. Tamilarasan, S. Thangavelu, *J. Mater. Sci. Mater. Electron.* **2021**, *32*, 4766.
- [78] X. Li, F. Qi, Y. Xue, C. Yu, H. Jia, Y. Bai, S. Wang, Z. Liu, J. Zhang, C. Tang, *RSC Adv.* **2016**, *6*, 99165.
- [79] S. Meng, X. Ye, X. Ning, M. Xie, X. Fu, S. Chen, *Appl. Catal. B Environ.* **2016**, *182*, 356.
- [80] B. Singh, K. Singh, M. Kumar, S. Thakur, A. Kumar, *Chem. Phys.* **2020**, *531*, 110659.
- [81] X.-F. Wu, H. Li, Y. Sun, Y.-J. Wang, C.-X. Zhang, J.-Z. Su, J.-R. Zhang, F.-F. Yang, Y. Zhang, J.-C. Pan, *Appl. Phys. A* **2017**, *123*, 709.
- [82] A. Biswas, S. Saha, N. R. Jana, *New J. Chem.* **2020**, *44*, 9278.
- [83] H. Xu, L. Liu, Y. Song, L. Huang, Y. Li, Z. Chen, Q. Zhang, H. Li, J. Alloys Compd. **2016**, *660*, 48.
- [84] U. Rafiq, M. Wahid, K. Majid, *ChemistrySelect* **2020**, *5*, 11637.
- [85] Q.-P. Zhang, D.-M. Liang, W.-F. Zhu, J.-H. Liu, Y. Wu, D.-G. Xu, X.-Y. Bai, M. Wei, Y.-L. Zhou, *J. Solid State Chem.* **2019**, *269*, 594.
- [86] X. Yao, C. Wang, H. Liu, H. Li, P. Wu, L. Fan, H. Li, W. Zhu, *Ind. Eng. Chem. Res.* **2019**, *58*, 863.
- [87] C. Huang, W. Ye, Q. Liu, X. Qiu, *ACS Appl. Mater. Interfaces* **2014**, *6*, 14469.
- [88] Y. Zhang, Y.-N. Wang, X.-T. Sun, L. Chen, Z.-R. Xu, *Sens. Actuators B Chem.* **2017**, *246*, 118.
- [89] J. Chen, J. Zhu, Z. Da, H. Xu, J. Yan, H. Ji, H. Shu, H. Li, *Appl. Surf. Sci.* **2014**, *313*, 1.
- [90] J. Wang, J. Shen, D. Fan, Z. Cui, X. Lü, J. Xie, M. Chen, *Mater. Lett.* **2015**, *147*, 8.
- [91] I. M. Patil, A. Swami, R. Chavan, M. Lokanathan, B. Kakade, *ACS Sustainable Chem. Eng.* **2018**, *6*, 16886.
- [92] M.-J. Lee, B. Ye, B. Jeong, S.-Y. Chun, T. Kim, D.-H. Kim, H. Lee, H.-D. Kim, *ACS Appl. Nano Mater.* **2020**, *3*, 11254.
- [93] X. Sun, Q. Zhu, X. Kang, H. Liu, Q. Qian, J. Ma, Z. Zhang, G. Yang, B. Han, *Green Chem.* **2017**, *19*, 2086.
- [94] Z. Liu, M. Zhang, H. Wang, D. Cang, X. Ji, B. Liu, W. Yang, D. Li, J. Liu, *ACS Sustainable Chem. Eng.* **2020**, *8*, 5278.
- [95] Y. Chen, J. Cai, P. Li, G. Zhao, G. Wang, Y. Jiang, J. Chen, S. X. Dou, H. Pan, W. Sun, *Nano Lett.* **2020**, *20*, 6807.
- [96] H. Moon, C. Lee, W. Lee, J. Kim, H. Chae, *Adv. Mater.* **2019**, *31*, 1804294.
- [97] B. Xie, H. Liu, R. Hu, C. Wang, J. Hao, K. Wang, X. Luo, *Adv. Funct. Mater.* **2018**, *28*, 1801407.
- [98] W. Wang, P. Deng, X. Liu, Y. Ma, Y. Yan, *Microchem. J.* **2021**, *162*, 105876.
- [99] I. M. Patil, M. Lokanathan, B. Kakade, *J. Mater. Chem. A* **2016**, *4*, 4506.
- [100] J. Ren, Q. Li, L. Yan, L. Jia, X. Huang, L. Zhao, Q. Ran, M. Fu, *Mater. Des.* **2020**, *191*, 108663.
- [101] J. Wang, F. Ma, W. Liang, R. Wang, M. Sun, *Nanophotonics* **2017**, *6*, 943.
- [102] Y. Jiang, X. Lin, T. Low, B. Zhang, H. Chen, *Laser Photonics Rev.* **2018**, *12*, 1800049.
- [103] J. Wang, F. Ma, M. Sun, *RSC Adv.* **2017**, *7*, 16801.
- [104] T. Huang, X. Zeng, Y. Yao, R. Sun, F. Meng, J. Xu, C. Wong, *RSC Adv.* **2016**, *6*, 35847.
- [105] T. Huang, X. Zeng, Y. Yao, R. Sun, F. Meng, J. Xu, C. Wong, *RSC Adv.* **2017**, *7*, 23355.
- [106] J. Yang, L.-S. Tang, R.-Y. Bao, L. Bai, Z.-Y. Liu, B.-H. Xie, M.-B. Yang, W. Yang, *Sol. Energy Mater. Sol. Cells* **2018**, *174*, 56.
- [107] F. Guo, X. Shen, J. Zhou, D. Liu, Q. Zheng, J. Yang, B. Jia, A. K. Lau, J. K. Kim, *Adv. Funct. Mater.* **2020**, *30*, 1910826.
- [108] Y. Fan, Z. Yang, W. Hua, D. Liu, T. Tao, M. M. Rahman, W. Lei, S. Huang, Y. Chen, *Adv. Energy Mater.* **2017**, *7*, 1602380.
- [109] J. Su, G.-D. Li, X.-H. Li, J.-S. Chen, *Adv. Sci.* **2019**, *6*, 1801702.
- [110] K.-X. Zhang, H. Su, H.-H. Wang, J.-J. Zhang, S.-Y. Zhao, W. Lei, X. Wei, X.-H. Li, J.-S. Chen, *Adv. Sci.* **2018**, *5*, 1800062.
- [111] M. Xu, T. Liang, M. Shi, H. Chen, *Chem. Rev.* **2013**, *113*, 3766.
- [112] O. L. Krivanek, M. F. Chisholm, V. Nicolosi, T. J. Pennycook, G. J. Corbin, N. Dellby, M. F. Murfitt, C. S. Own, Z. S. Szilagy, M. P. Oxley, S. T. Pantelides, S. J. Pennycook, *Nature* **2010**, *464*, 571.
- [113] L. Ci, L. Song, C. Jin, D. Jariwala, D. Wu, Y. Li, A. Srivastava, Z. F. Wang, K. Storr, L. Balicas, F. Liu, P. M. Ajayan, *Nat. Mater.* **2010**, *9*, 430.
- [114] C. Huang, C. Chen, M. Zhang, L. Lin, X. Ye, S. Lin, M. Antonietti, X. Wang, *Nat. Commun.* **2015**, *6*, 7698.
- [115] P. Sutter, R. Cortes, J. Lahiri, E. Sutter, *Nano Lett.* **2012**, *12*, 4869.
- [116] W. K. Darkwah, Y. Ao, *Nanoscale Res. Lett.* **2018**, *13*, 388.
- [117] H. Xu, Z. Wu, Y. Wang, C. Lin, *J. Mater. Sci.* **2017**, *52*, 9477.
- [118] L. Acharya, S. Nayak, S. P. Pattnaik, R. Acharya, K. Parida, *J. Colloid Interface Sci.* **2020**, *566*, 211.
- [119] Z. He, C. Kim, L. Lin, T. H. Jeon, S. Lin, X. Wang, W. Choi, *Nano Energy* **2017**, *42*, 58.
- [120] L. Acharya, S. P. Pattnaik, A. Behera, R. Acharya, K. Parida, *Inorg. Chem.* **2021**, *60*, 5021.
- [121] T. Wang, X. Liu, Q. Men, C. Ma, Y. Liu, Z. Liu, P. Huo, C. Li, Y. Yan, *J. Mol. Liq.* **2018**, *268*, 561.
- [122] A. K. Geim, I. V. Grigorieva, *Nature* **2013**, *499*, 419.
- [123] Y. Liu, N. O. Weiss, X. Duan, H.-C. Cheng, Y. Huang, X. Duan, *Nat. Rev. Mater.* **2016**, *1*, 16042.
- [124] Z. Liu, L. Song, S. Zhao, J. Huang, L. Ma, J. Zhang, J. Lou, P. M. Ajayan, *Nano Lett.* **2011**, *11*, 2032.
- [125] Q. Li, Z. Zhao, B. Yan, X. Song, Z. Zhang, J. Li, X. Wu, Z. Bian, X. Zou, Y. Zhang, Z. Liu, *Adv. Mater.* **2017**, *29*, 1701325.
- [126] C. Zhang, S. Zhao, C. Jin, A. L. Koh, Y. Zhou, W. Xu, Q. Li, Q. Xiong, H. Peng, Z. Liu, *Nat. Commun.* **2015**, *6*, 6519.
- [127] Z. Zhang, X. Ji, J. Shi, X. Zhou, S. Zhang, Y. Hou, Y. Qi, Q. Fang, Q. Ji, Y. Zhang, M. Hong, P. Yang, X. Liu, Q. Zhang, L. Liao, C. Jin, Z. Liu, Y. Zhang, *ACS Nano* **2017**, *11*, 4328.
- [128] T. Szkopek, *Nat. Nanotechnol.* **2021**, *16*, 853.
- [129] L. Wu, A. Wang, J. Shi, J. Yan, Z. Zhou, C. Bian, J. Ma, R. Ma, H. Liu, J. Chen, Y. Huang, W. Zhou, L. Bao, M. Ouyang, S. J. Pennycook, S. T. Pantelides, H.-J. Gao, *Nat. Nanotechnol.* **2021**, *16*, 882.
- [130] L. Liu, C. Liu, L. Jiang, J. Li, Y. Ding, S. Wang, Y.-G. Jiang, Y.-B. Sun, J. Wang, S. Chen, D. W. Zhang, P. Zhou, *Nat. Nanotechnol.* **2021**, *16*, 874.
- [131] C. R. Woods, P. Ares, H. Nevison-Andrews, M. J. Holwill, R. Fabregas, F. Guinea, A. K. Geim, K. S. Novoselov, N. R. Walet, L. Fumagalli, *Nat. Commun.* **2021**, *12*, 347.
- [132] K. Yao, N. R. Finney, J. Zhang, S. L. Moore, L. Xian, N. Tancogne-Dejean, F. Liu, J. Ardelean, X. Xu, D. Halbertal, K. Watanabe, T. Taniguchi, H. Ochoa, A. Asenjo-Garcia, X. Zhu, D. N. Basov, A. Rubio, C. R. Dean, J. Hone, P. J. Schuck, *Sci. Adv.* **2021**, *7*, eabe8691.



Junkai Ren obtained his B.E. degree in materials forming and control engineering from Changsha University of Science and Technology (CSUST, China), in 2015 and received his M.S. degree in chemistry and physics of polymers from University of Chinese Academy of Sciences (UCAS, China), in 2018. He now is a Ph.D. student in chemical sciences and technologies in University of Sassari and Cagliari (UniSS-UniCA, Italy). Currently, he works at the Laboratory of Materials Science and Nanotechnologies (LMNT) to explore the optical properties of boron nitride nanomaterials and developing functional applications based on their nanocomposites.



Plinio Innocenzi is full professor of materials science and technology and director of the Laboratory of Materials Science and Nanotechnology at the University of Sassari in Italy. He has served as science and technology counsellor at the Embassy of Italy in China from 2010 to 2018. He is a fellow of the Royal Society of Chemistry, honorary professor of the Luoyang Normal University and has published more 220 articles in sol-gel chemistry, self-assembly of nanomaterials, carbon dots, and 2D materials. He has published several books on sol-gel chemistry and science popularization.